The Astrophysical Journal Letters, 874:L8 (10pp), 2019 March 20 https://doi.org/10.3847/2041-8213/ab0e8d

TESS Habitable Zone Star Catalog

L. Kaltenegger[1], J. Pepper[2], K. Stassun[3], and R. Oelkers[3]
[1] Carl Sagan Institute, Cornell University, Space Science Institute 312, Ithaca, NY 14850 USA; lkaltenegger@astro.cornell.edu
[2] Lehigh University, Physics Department, Bethlehem, PA 18015, USA
[3] Vanderbilt University, Physics & Astronomy Department, Nashville, TN 37235, USA
Received 2018 November 7; revised 2019 February 5; accepted 2019 February 19; published 2019 March 26

Abstract

We present the *Transiting Exoplanet Survey Satellite* (*TESS*) Habitable Zone Stars Catalog, a list of 1822 nearby stars with a *TESS* magnitude brighter than $T = 12$ and reliable distances from *Gaia* DR2, around which the NASA's *TESS* mission can detect transiting planets, which receive Earth-like irradiation. For all those stars *TESS* is sensitive down to 2 Earth radii transiting planets during one transit. For 408 stars *TESS* can detect such planets down to 1 Earth-size during one transit. For 1690 stars, *TESS* has the sensitivity to detect planets down to 1.6 times Earth-size, a commonly used limit for rocky planets in the literature, receiving Earth-analog irradiation. We select stars from the *TESS* Candidate Target List, based on *TESS* Input Catalog Version 7. We update their distances using *Gaia* Data Release 2, and determine whether the stars will be observed for long enough during the 2 yr prime mission to probe their Earth-equivalent orbital distance for transiting planets. We discuss the subset of 227 stars for which *TESS* can probe the full extent of the Habitable Zone, the full region around a star out to about a Mars-equivalent orbit. Observing the *TESS* Habitable Zone Catalog Stars will also give us deeper insight into the occurrence rate of planets, out to Earth-analog irradiation as well as in the Habitable Zone, especially around cool stars. We present the stars by decreasing angular separation of the 1 au equivalent distance to provide insights into which stars to prioritize for ground-based follow-up observations with upcoming extremely large telescopes.

Key words: astrobiology – astronomical databases – catalogs – planets and satellites: detection – planets and satellites: terrestrial planets – stars: general

Supporting material: machine-readable tables

1. Introduction

Several thousand extrasolar planets have already been detected orbiting a variety of host stars and provide a first glimpse of the diversity of other worlds (e.g., reviewed in Udry & Santos 2017; Winn & Fabrycky 2015; Kaltenegger 2017). Among them, the first dozens of potentially habitable planets have been identified (see, e.g., review by Kaltenegger 2017). Previous ground-based wide-field transit surveys like WASP, TrES, HATNet, KELT, XO, and QES (Alonso et al. 2004; Bakos et al. 2004; McCullough et al. 2005; Pollacco et al. 2006; Pepper et al. 2007; Alsubai et al. 2013) have been able to detect mostly gaseous planets, while dedicated space-based surveys like *CoRoT* (Auvergne et al. 2009) and *Kepler* (Borucki et al. 2010) have been designed to only survey a small region of the sky with high precision.

In contrast, the new *Transiting Exoplanet Survey Satellite* (*TESS*) is designed to search the whole sky for extrasolar planets and also to search for potentially habitable exoplanets around the closest and brightest stars. *TESS* is a NASA Explorer space mission with four wide-field cameras, and combines the advantage of wide-field surveys with the photometric precision and long intervals of uninterrupted observation from space. However, in order to complete the survey within the primary mission time of two years, *TESS* will monitor stars for 27 days near the ecliptic, with overlapping sectors yielding observational time baselines of up to almost a year near the ecliptic pole, in a region that overlaps with the *James Webb Space Telescope* (*JWST*) continuous observing zone (Ricker et al. 2016). *TESS* monitors several hundred thousand Sun-like and smaller stars for transiting planets and prioritizes bright stars, which allow detailed follow-up measurements of properties including planetary mass and atmospheric composition. *TESS* has published its first detected planets (see, e.g., Huang et al. 2019; Vanderspeck et al. 2019).

For which of the 200,000–400,000 stars selected for exoplanet observations in the *TESS* Input Target Catalog could *TESS* detect planets like our own? Here we present the *TESS* Habitable Zone Star Catalog: our catalog lists the stars for which *TESS* can detect planets that receive equivalent irradiation as Earth. For a subset of these stars *TESS* can detect planets in the whole Habitable Zone (HZ). We use the *TESS* Input Catalog (TIC; Stassun et al. 2018) as the basis for our analysis, and update the distances with *Gaia* Data Release 2 (DR2; Gaia Collaboration et al. 2018). What distinguishes this catalog from previous work like HabCat (Turnbull & Tarter 2003), DASSC (Kaltenegger et al. 2010), and CELESTA (Chandler et al. 2016) is that the stars included here are specifically selected to have sufficient observation time by *TESS* for transit detection out to the Earth-equivalent orbital distance. We also use *Gaia* DR2 data, which allows us to exclude giant stars from the star sample and provides reliable distances for our full star sample. All the stars have been included in the *TESS* exoplanet Candidate Target List, ensuring that they will also have a 2 minute cadence observation (provided they do not fall in *TESS* camera pixel gaps), providing a specific catalog for the *TESS* mission of stars where planets in the Habitable Zone can be detected by *TESS*. This data will be available to the community in the ongoing public *TESS* data releases.

Several studies have explored the occurrence rate of planets from the known planets around different host stars (see the recent review in Kaltenegger 2017) and reach different conclusions. Simulations for the projected *TESS* planet yield

have been discussed in detail in previous papers (Sullivan et al. 2015; Barclay et al. 2018; Bouma et al. 2017; Huang et al. 2018) based on a range of assumptions for planet occurance rate (see Section 4.3). Note that we do not make assumptions about the planet occurrence rate here, and instead focus on the stars around which *TESS* can detect two transits for a planet receiving Earth-analog irradiation in its prime mission observation time. Observing the *TESS* Habitable Zone Catalog Stars will give us deeper insight into the occurrence rate of planets out to Earth-analog irradiation as well as in the Habitable Zone, informing the occurrence rate discussion for planets around cool stars.

Section 2 describes the Habitable Zone concept we use in our analysis, how we derived our catalog from the TIC-7, and how we updated the stellar distances using *Gaia* DR2, how we eliminated giant stars from the catalog and how we model detectability of transiting planets with different sizes. Section 3 presents the results and explores for how many stars *TESS* can probe the whole HZ, as well as for how many stars *TESS* can detect planets receiving Earth irradiation as a function of their size and which are in the *JWST* continuous and extended viewing zone. Section 4 discusses our results.

2. Methods

We first identify the stars for which *TESS* can detect planets out to the orbital region with similar top of the atmosphere flux as Earth receives, using the luminosity of the star to calculate the 1 au equivalent orbital distance from the star. This calculation is independent of models of a planet.

2.1. Habitable Zone Limits Used

We then analyze for how many stars *TESS* can observe two transits of planets with orbital periods that place them within the HZ of their star. The HZ is a tool that guides missions and surveys in prioritizing planets for time-intensive follow-up observations.

The HZ is defined as the region around one or multiple stars in which liquid water could be stable on a rocky planet's surface (e.g., Kasting et al. 1993; Kaltenegger & Haghighipour 2013; Kane & Hinkel 2013), facilitating the detection of possible atmospheric biosignatures. Although planets located outside the HZ are not excluded from hosting life, detecting biosignatures remotely on such planets should be extremely difficult. Liquid surface water is used because it remains to be demonstrated whether subsurface biospheres, for example, under an ice layer on a frozen planet, can modify a planet's atmosphere in ways that can be detected remotely.

The width and orbital distance of a given HZ depends to a first approximation on two main parameters: incident stellar flux and planetary atmospheric composition. The incident stellar flux depends on stellar luminosity, stellar spectral energy distribution, eccentricity of the planetary orbit, and the planet's orbital distance (semimajor axis). The warming due to atmospheric composition depends on the planet's atmospheric makeup, energy distribution, and resulting albedo and greenhouse warming. In the literature, very different values of stellar irradiance are used as boundaries for the HZ. Here we use the empirical habitable zone boundaries, which were originally defined using a 1D climate model by Kasting et al. (1993), and updated in Kopparapu et al. (2013), Ramirez & Kaltenegger (2016, 2017), for main-sequence (MS) stars with effective temperatures ($T_{\rm eff}$) between 2600 and 10,000 K. Table 1 provides values to estimate the size of the HZ, and also includes HZ limits based on 3D atmospheric models for our Sun (Leconte et al. 2013) for different host stars (Ramirez & Kaltenegger 2014) for comparison.

Table 1
Constants to Compute the Empirical Boundaries of the Habitable Zone Using Equation (1) (Kopparapu et al. 2013; Ramirez & Kaltenegger 2016)

Constants	Recent Venus Limit Inner Edge	3D Model Limit Inner Edge	Early Mars Limit Outer Edge
$S_{\rm Sun}$	1.7665	1.1066	0.324
A	1.3351e−4	1.2181e−4	5.3221e−5
B	3.1515e−9	1.534e−8	1.4288e−9
C	−3.3488e−12	−1.5018e−12	−1.1049e−12

Equation (1) gives a third-order polynomial curve fit of the modeling results for A- to M-type host stars as shown in Kaltenegger (2017) based on values derived from models by Kasting et al. (1993) and Kopparapu et al. (2013, 2014) and an extension of that work to 10,000 K by Ramirez & Kaltenegger (2016):

$$S_{\rm eff} = S_{\rm Sun} + a \cdot T^* + b \cdot T^{*2} + c \cdot T^{*3}, \quad (1)$$

where $T^* = (T_{\rm eff} - 5780)$ and $S_{\rm Sun}$ is the stellar incident values at the HZ boundaries in our solar system. Table 1 shows the constants to derive the stellar flux at the HZ limits valid for $T_{\rm eff}$ between 2600 and 10,000 K: the inner boundaries of the empirical HZ Recent Venus (RV) as well as an alternative inner edge limit modeled by 3D Global Climate model (3D; Leconte et al. 2013) and the outer limits Early Mars (EM). Note that the inner limit of the empirical HZ is not well known because of the lack of a reliable geological surface history of Venus beyond about 1 billion years due to resurfacing of the stagnant lid, which allows for the possibility of a liquid surface ocean; however, it does not stipulate a liquid ocean surface. Climate models also show limitations due to unknown cloud feedback for higher stellar irradiation. Therefore, we concentrate on the Earth-equivalent orbital distance in this paper and use the empirical HZ limits as an example for an orbital distance range. The outer HZ limit is comparable in the 3D and 1D model and are therefore not given in separate columns in Table 1. The orbital distance of the HZ boundaries can be calculated from $S_{\rm eff}$ using Equation (2):

$$d = \sqrt{\frac{L/L_{\rm Sun}}{S_{\rm eff}}}, \quad (2)$$

where $L/L_{\rm Sun}$ is the stellar luminosity in solar units and d is the orbital distance in astronomical units.

Models of the Habitable Zone take into account that cool red stars, which have a stellar energy distribution that peaks at a redder wavelength than the Sun, heat the surface of an Earth-like planet more effectively. This effect is not included when calculating the 1 au equivalent distance, but it is included in atmospheric models, which generated the concept of the Habitable Zone. The stellar energy distribution depends on spectral type and changes with age. A star's radiation shifts to longer wavelengths with cooler surface temperatures, which makes the light of a cooler star more efficient at heating an

Earth-like planet with a mostly N_2–H_2O–CO_2 atmosphere (see, e.g., Kasting et al. 1993). This is partly due to the effectiveness of Rayleigh scattering, which decreases at longer wavelengths. A second effect is the increase in NIR absorption by H_2O and CO_2 as the star's spectral peak shifts to these wavelengths, meaning that the same integrated stellar flux that hits the top of a planet's atmosphere from a cool red star warms a planet more efficiently than the same integrated flux from a star with a higher effective surface temperature. Stellar luminosity as well as the SED change with stellar spectral type and age, which influences the orbital distance at which an Earth-like planet can maintain climate conditions that allow for liquid water on its surface (see review by Kaltenegger 2017).

2.2. *How the* TESS *Habitable Zone Star Catalog was Created*

We base our analysis on version 7 of the *TESS* Input Catalog (TIC-7) and the accompanying Candidate Target List (CTL-7.02), described in Stassun et al. (2018) and in the TIC Data Release Notes.[4] The TIC includes all stars in the sky down to the magnitude limits of all-sky photometric catalogs, most significantly 2MASS. Stars in the CTL are selected as high-quality targets for *TESS* observations, consisting primarily of bright, cool, dwarf stars. CTL-7 contains roughly 3.75 million stars, of which approximately 400,000 will ultimately be selected as *TESS* 2 minute observing targets for transit searches. The physical parameters of the stars in the CTL are compiled from a variety of catalogs, and also calculated using a set of empirical relations, all described in Stassun et al. (2018). Those physical parameters include the stellar temperatures, masses, radii, and luminosities.

Since CTL-7.02 was assembled, the second data release from the *Gaia* mission (*Gaia* DR2) became available (Gaia Collaboration et al. 2016, 2018). The release includes updates to parallaxes for nearly all stars in the CTL. As discussed by Bailer-Jones (2015), the simple $1/\pi$ distance estimator becomes sensitive to the assumed prior when the relative uncertainty in the parallax is larger than ≈20%. While the majority of the stars in our sample satisfy this criterion, for completeness we elected to adopt distances for all of the stars using an explicit Bayesian prior. Specifically, we use the distance estimates from Bailer-Jones et al. (2018), which invokes a weak prior based on a simple Milky Way model for the stellar density distribution as a function of Galactocentric radius and height above the Galactic plane.

Following Sullivan et al. (2015), we first use a T-mag cutoff to limit our sample. For faint stars, it will be more difficult to detect their transits, to obtain dynamical confirmation of any planets around them, or to probe the atmospheres of such planets. To identify the T-mag cutoff, we selected a star with $T_{\rm eff} = 3500$ K as our fiducial star, just as Sullivan selected a star with $T_{\rm eff} = 3200$ K. Our choice differs from Sullivan because those authors did not have access to the actual TIC and CTL. We are able to identify $T_{\rm eff} = 3500$ K as the most common $T_{\rm eff}$ for a cool star in the CTL. At that $T_{\rm eff}$, the stellar radius is $0.37 R_{\rm Sun}$, and a transit of an Earth-sized planet around a star that size would yield a transit depth of 600 ppm. Following the same procedure as Sullivan, we then set the T-mag limit to correspond to the magnitude where the per-point photometric precision of *TESS* is equal to the fiducial transit depth, which for 600 ppm is $T = 12$.

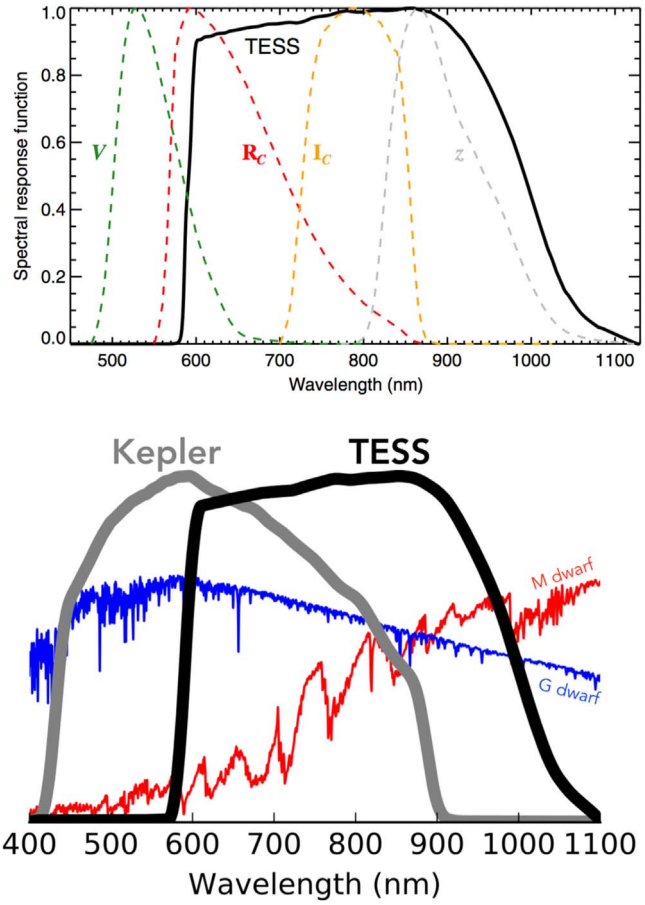

Figure 1. Top panel: *TESS* spectral response function (black line), defined as the product of the long-pass filter transmission curve and the detector quantum efficiency curve. Johnson–Cousins V, R_C, and I_C filter curves and the Sloan Digital Sky Survey z filter curve. Each of the functions has been scaled to have a maximum value of unity. Image credit: Ricker et al. (2016). Bottom panel: *TESS* bandpass compared to *Kepler* (Image credit: Zach Berta-Thompson with data from Sullivan et al. 2015).

The *TESS* photometric bandpass is very broad (see Figure 1, Ricker et al. 2016; Sullivan et al. 2015). *TESS* will monitor a much larger sample of M stars compared to *Kepler*, thus the bandpass extends further to red wavelengths. It is broadly similar to a Cousins I-band filter. As shown in Figure 1, stars with different $T_{\rm eff}$ can have similar T-mag. Thus our catalog provides targets for a wide range of ground- and space-based telescopes, which are optimized for different wavelengths.

A number of empirical relations have been defined (Stassun et al. 2018) for conversion to T magnitude from many other standard filters and systems. To provide a very crude sense of the relationship between the *TESS* and *Gaia* magnitudes for the entire TIC, $T = G - 0.5$ with a scatter of <1 mag; that is, T is on average roughly one-half magnitude brighter than G.

We then calculate how long each of the CTL stars would be observed by *TESS* in the prime 2 yr mission. We use a parameterized estimate (Barclay et al. 2018) based on the ecliptic latitude of the stars to calculate the average number of *TESS* sector observations each star would receive. For each star, we calculate the Earth-equivalent orbital distance based on the star's luminosity and the corresponding orbital period. We then analyze whether the star would be observed for long

[4] https://docs.google.com/document/d/1BQ4txZ5YmTMwNLiI5ilc-YHkYZqAMCg5HHFaTLoI33w/edit?usp=sharing

enough by *TESS* for the detection of two transits for a planet at that orbital distance. Furthermore we calculate different limits of the HZ as described in Section 2.1 and redo our analysis for the concept of the empirical HZ.

2.3. Redetermination of Radii and Identification of Red Giant Contaminants Using Gaia DR2 Data

To identify evolved stars in our initial CTL-7 sample, we use the *Gaia* DR2 data to update the distance and radii assumed in CTL-7. 57 stars in our initial CTL-7 sample do not have reported *Gaia* DR2 parallaxes, and we were unable to match them to any *Gaia* source; these 57 stars in general appear to have very high proper motions (>100 mas yr^{-1}). Due to the unknown distance we remove these 57 stars from our analysis. We retain the effective temperatures from the current CTL-7 but apply the *Gaia* DR2 based distance estimator from Bailer-Jones et al. (2018) to rederive the stellar radii for our sample. This enables a more robust elimination of evolved stars from the sample. Current CTL-7 includes a likely contamination by red giants of about 2%, or about 30 stars in the sample used in this paper. We use the *Gaia* DR2 distances and recalculated the stellar radii from the *Gaia* DR2 G magnitudes, the *Gaia* bolometric correction (BC_G) computed from the effective temperature (according to Andrae et al. 2018), and the distance (Bailer-Jones et al. 2018).

The BC_G relation is formally valid only for $T_{\rm eff} > 3300$ K; therefore, for stars whose temperatures had been estimated in the TIC-7 from the specially curated Cool Dwarf List (Muirhead et al. 2018; Stassun et al. 2018), we retained the stellar radius originally determined in the CTL; these are cool stars with high proper motions and therefore should be reliably nearby cool dwarfs.

Figure 2 shows our sample in the radius versus temperature plane, where the radii have been updated from the CTL-7 as described above. The vast majority of the sample follows the expected relationship for MS cool dwarfs. However, a small number of stars have much larger radii; these are evolved stars that were incorrectly labeled as dwarfs in CTL-7. A cutoff of 1.5 $R_{\rm Sun}$ effectively demarcates these evolved stars beyond the scatter in the MS population. The figure also highlights stars whose *Gaia* DR2 based distances are 300 pc or beyond, which principally identifies the same evolved stars with radii larger than 1.5 $R_{\rm Sun}$, but also identifies three additional stars that were putative cool dwarfs but are evidently at large distances such that they must be more luminous (i.e., larger) than expected. There are 35 stars in our sample that are identified as evolved stars by these criteria.

As a consistency check, we compare our derived stellar radii with those reported in the *Gaia* DR2 database for 813 of the stars in our sample (*Gaia* DR2 includes radius estimates for only about half of our sample). The agreement overall is excellent, except again for a small number of outliers already identified above. In addition, we note that the radii of the coolest stars are in general overestimated by *Gaia* DR2, which is expected given the limitations of the *Gaia* DR2 stellar properties pipeline at temperatures below about 3500 K (Andrae et al. 2018). Figure 2 (right) shows how the radii newly determined in this paper compare to those from the original TIC. While planets orbiting evolved host stars might also host habitable planets (see, e.g., Ramirez & Kaltenegger 2017), due to the short time a planet can spend in the RG HZ, we excluded RGs from our catalog.

In summary, we have verified that nearly all of our selected sample indeed consists of cool dwarf stars, based on radius estimates updated from the CTL using the newly available *Gaia* DR2 parallaxes. We are able to eliminate 35 stars as being more evolved (having larger radii) than had been estimated in the TIC-7; these 35 stars constitute about 2% of our sample, consistent with the TIC-7 contamination by red giants of 2% (Stassun et al. 2018). Here we identify and remove these evolved contaminants by requiring $R_{\rm star} < 1.5$ $R_{\rm Sun}$ and $d < 300$ pc, leaving a final analysis sample of 1822 cool, nearby dwarfs.

2.4. Which Planet Sizes Can TESS Detect during One Transit?

To analyze which planets *TESS* can detect during one planetary transit, we first calculate the maximum transit time for each planet at the Earth-equivalent orbital distance around each of the stars in the *TESS* Habitable Zone Star Catalog. To estimate the noise, we adopted the approximate polynomial form of the *TESS* noise model from Oelkers et al. (2018). This is a slightly updated version of the original *TESS* noise model from Sullivan et al. (2015), and uses the prelaunch systematic noise floor of 60 ppm hr$^{-0.5}$. Using the maximum transit time of each planet at the Earth-equivalent orbital distance for their host star, we analyze whether *TESS* can detect a transiting planet of a certain size during one transit, with the minimum requirement being that the planet's signal is the same strength as the noise signal. We assume different sizes for the hypothetical planets between 1 and 2 Earth radii for our analysis. Note that the number of stars around which *TESS* can detect transiting planets of a certain size is not the same as the number of planets we expect to find because the number of expected planet detections depend among different factors on the intrinsic occurrence rate of small planets in the habitable zones of these stars, the alignment of such planets orbiting stars in the sample we have presented, and the characteristics of the *TESS* data that would allow such transiting planets to be confidently detected, most with a small number of transits seen (see discussion in Section 4.3).

3. Results

3.1. For How Many Stars Can TESS Find Planets at Earth-equivalent Distance?

TESS can detect two transits of a planet orbiting at the 1 au equivalent distance for 1822 stars brighter than $T = 12$ during its prime mission. The effective temperatures of these stars are roughly between about 2700 and 5400 K, with distances up to about 300 pc. The top panel of Figure 3 shows the distribution of the *TESS* Habitable Zone stars on the sky, with a strong concentration around the ecliptic poles, where the *TESS* observational sectors overlap and allow for longer observation times. The size of the circles indicate the *TESS* magnitude with larger circles representing stars with higher apparent brightness.

The *TESS* Habitable Zone Stellar Catalog is populated by cool stars, which reflects the decrease of the Earth-equivalent orbital distance with decreasing luminosity of the star. The period of planets orbiting cool stars at these orbital distances are short enough so that two transits can be detected during the nominal *TESS* observation time of these stars. Due to *TESS*'s observing strategy, *TESS* Habitable Zone Catalog stars with higher effective surface temperature are located in the regions

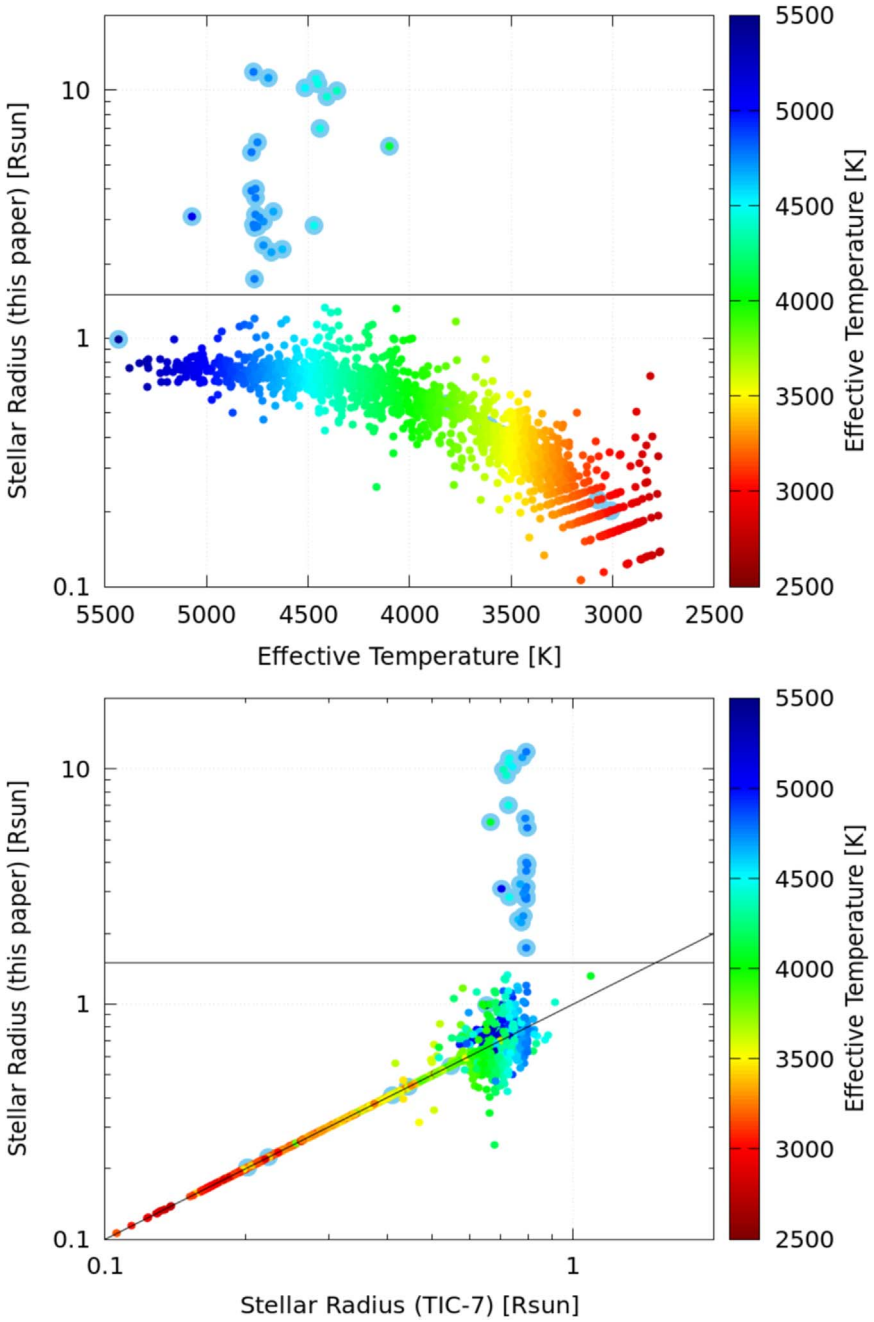

Figure 2. Stellar radius vs. (top) effective temperature for our TIC-7 study sample. The effective temperatures are taken from the CTL but the radii are updated from the CTL using the newly available *Gaia* DR2 parallaxes. Highlighted in blue are evidently evolved stars that we identify and eliminate as $R_{\rm star} < 1.5\ R_{\rm Sun}$ or $d > 300$ pc. (bottom) The stellar radii in this Letter are compared against the stellar radii as originally reported in TIC-7. The color bar represents the effective stellar temperature.

around the ecliptic pole, where the observing segments overlap and allow for longer observations. 137 of the stars of the *TESS* Habitable Zone Catalog are located in the *JWST* continuous viewing zone, which is located ±5° from the ecliptic poles. These stars have effective temperatures between 3000 and 5200 K and distances up to about 230 pc, indicated in Table 2 with the tag "*JWST*." Out to 20° off the pole, *JWST* can observe a star for a minimum of 250 days out of a year. 1350 stars of the *TESS* Habitable Zone Star catalog are located within 20° from the ecliptic poles (see Figure 3 for the subset of stars which are (third row) in the continuous viewing zone and (bottom) in the 250 day observation viewing zone of *JWST*).

Table 2 lists the stars sorted by decreasing apparent separation of the 1 au equivalent orbital distance as seen from Earth in milliarcseconds (mas). The column called "Sector" shows whether the star has already been observed with *TESS* in Sectors 1 through 4. The catalog can be downloaded under filtergraph/ https://filtergraph.com/tess_habitable_zone_catalog.

3.2. *For How Many Stars Can* TESS *Detect Planets in the Whole Habitable Zone?*

For 227 stars brighter than $T = 12$, *TESS* can detect two transits of a planet through the whole empirical Habitable

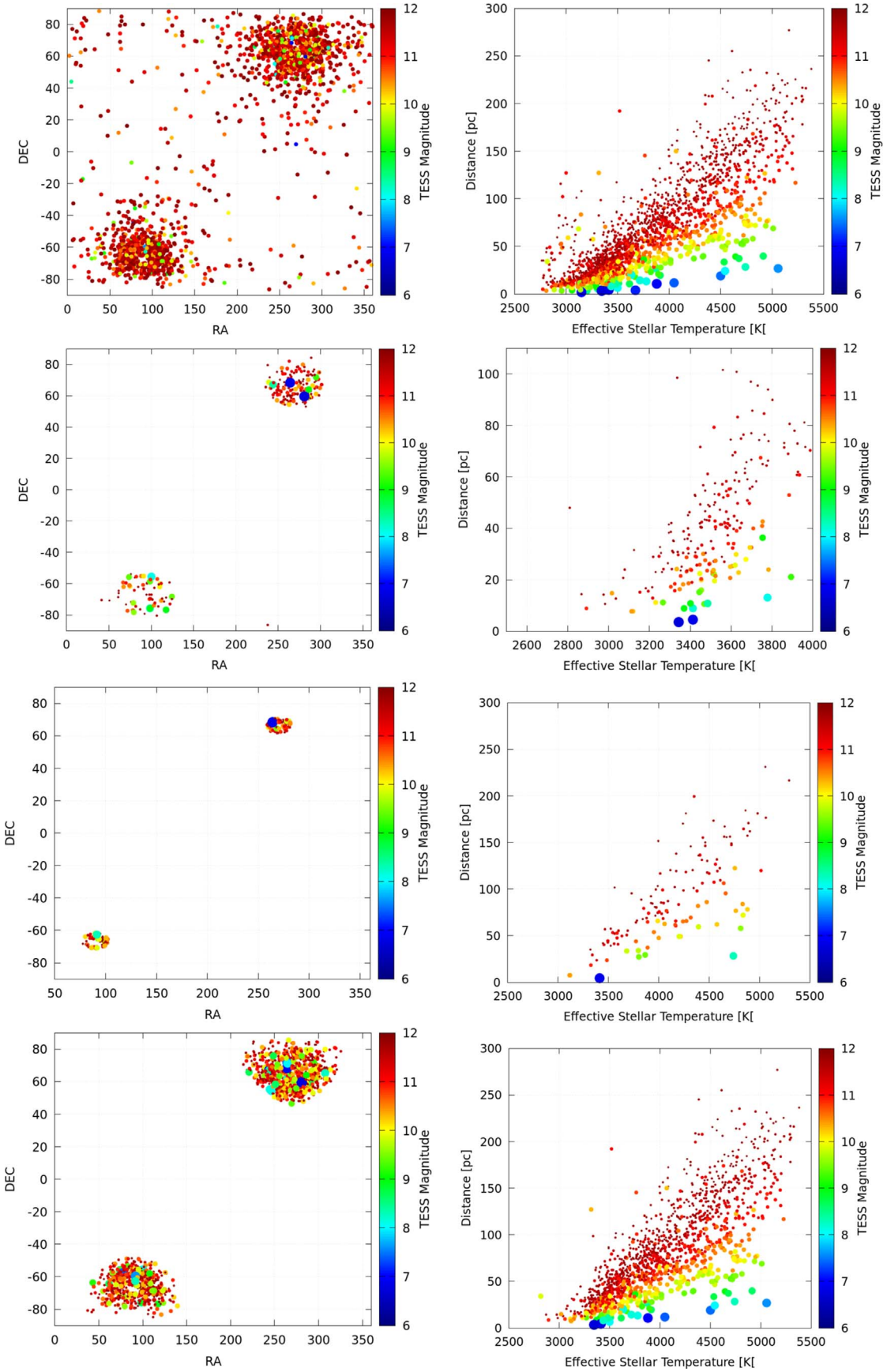

Figure 3. (Left) Distribution and (right) distance of these stars from the Sun vs. effective stellar temperature of the stars on the sky where *TESS* can detect planets (top) out to the 1 au equivalent distance and (second row) throughout the whole empirical HZ (third row) *JWST* continuous viewing area and (bottom) a 250 day *JWST* viewing zone.

Table 2
Stars where *TESS* can Detect Planets Out to the 1 au Equivalent Distance, Sorted by Decreasing Apparent Angular Separation in Milliarcsec (mas), the Full Table is Available Online[a]

Name
Temperature
TESS mag
Distance
Observing Time
Orbital Separation
Orbital Period
Coordinates
Apparent Angular Separation
Transit Time
Gaia Name
2MASS Name
HZ
JWST
Transit Earth
TESS Sectors

Note.
[a] TIC_ID *TESS* input catalog ID, lat latitude, Gaia_ID *Gaia* catalog ID, TWO_MASS_ID *Two* Micron All Sky Survey catalog ID, RV Recent Venus, EA Earth Analog, EM Early Mars, S observed sector of the *TESS* mission (S1 = sector 1), *JWST* star is in the *JWST* continuous viewing zone, HZ *TESS* can probe the full HZ for transiting planets, detect for one transit *TESS* can detect a 1 Earth-size planet during one transit, comment: yes = 1, no = 0.

(This table is available in its entirety in machine-readable form.)

Table 3
Stars where *TESS* can Detect Planets throughout the Empirical HZ, Sorted by Decreasing Apparent Angular Separation in Milliarcsec (Subset of Table 2), Full Table is Available Online[a]

Name
Temperature
TESS mag
Distance
Observing Time
Orbital Separation
Orbital Period
Coordinates
Apparent Angular Separation
Transit Time
Gaia Name
2MASS Name
HZ
JWST
Transit Earth
TESS Sectors

Note.
[a] TIC_ID *TESS* input catalog ID, lat latitude, Gaia_ID *Gaia* catalog ID, TWO_MASS_ID *Two* Micron All Sky Survey catalog ID, RV Recent Venus, EA Earth Analog, EM Early Mars, S observed sector of the *TESS* mission (S1 = sector 1), *JWST* star is in the *JWST* continuous viewing zone, HZ *TESS* can probe the full HZ for transiting planets, detect for one transit *TESS* can detect a 1 Earth-size planet during one transit, comment: yes = 1, no = 0.

(This table is available in its entirety in machine-readable form.)

Zone, planets receiving stellar irradiation comparable to RV to EM equivalent. Probing the whole Habitable Zone will give us a deeper understanding of the environment, formation, and distribution of planets in the Habitable Zone of stars. These 227 stars have effective temperatures between about 2800 and 4000 K for distances up to about 100 pc. The second row of Figure 3 shows the distribution of these stars by distance based on *Gaia* DR2 data and the distribution of the stars in ecliptic latitude. Table 3 shows this specific subset of the stars in Table 2, the stars for which *TESS* can probe the whole HZ for transiting planets, sorted by decreasing apparent separation of the outer limit of the empirical HZ in mas, indicated in Table 2 with the tag "HZ."

3.3. For How Many Stars Can TESS Detect a Small Planet Receiving Earth-like Irradiation?

For 408 of the *TESS* HZ catalog stars, *TESS* has the sensitivity to detect a 1 Earth-size planet orbiting at the 1 au-equivalent distance, with a minimum requirement that the transiting planetary signal is bigger than the noise signal during one transit. For 1690 stars *TESS* can detect a planet with 1.6 Earth radii and for all 1822 stars *TESS* can detect a planet of 2 Earth radii or larger during one transit. The boundary between rocky and gaseous planets is not well understood yet; commonly values between 1.6 and 2 Earth radii are used as boundaries between rocky and gaseous planets (see, e.g., Rogers 2015; Wolfgang et al. 2016 and a discussion in Kaltenegger 2017). Figure 4 shows the transit signal for the subset of stars, where *TESS* can detect (a) a 1 Earth-size planet during one transit and (b) the full set of stars for which *TESS* can detect 2 Earth-size planet. Note that adding transit observation will increase the transit signal while requiring a specific signal-to-noise ratio will change the number of stars *TESS* can probe for transiting planets as well (see detailed discussion in Section 4.3).

3.4. Prospects for Follow-up Characterization of TESS Planets

Due to the wide range of effective surface temperatures of the stars in the *TESS* HZ catalog, which uses a Tmag cutoff, a wide range of telescopes can provide follow-up observations for different subsets of stars—e.g., instruments optimized for cool red stars would be optimized for the cool star in our catalog.

As discussed in detail in Sullivan et al. (2015) and Ricker et al. (2016), follow-up observations will allow characterization of *TESS* planets. Because of the short periods, even low-mass planets—we have assumed 1 Earth mass planets for our calculations shown in Figure 4—produce a radial-velocity semiamplitude K between 50 and 0.5 m s^{-1} putting them within reach of current and upcoming spectrographs. Note that these values are a conservative estimate because they increase with planetary mass and rocky planet models predict 10 Earth masses for a 2 Earth radii planet.

Ground-based facilities and upcoming space-based facilities such as CHEOPS (Fortier et al. 2014) could use photometry to look for transit timing variations to improve estimates of relative planetary mass. Asteroseismology using data from *TESS* or the upcoming PLATO mission (Rauer et al. 2014) could further constrain the stellar radii.

The prospects for follow-up atmospheric characterization with *JWST* have been detailed by several teams (e.g., Clampin et al. 2009; Deming et al. 2009; Kaltenegger & Sasselov 2010; Kempton et al. 2018). Note that the *TESS* HZ catalog is focused on *TESS*'s sensitivity to planets between 1 and 2 Earth radii receiving similar insolation to present-day Earth. Thus the nominal calculations for planets using hydrogen atmospheres

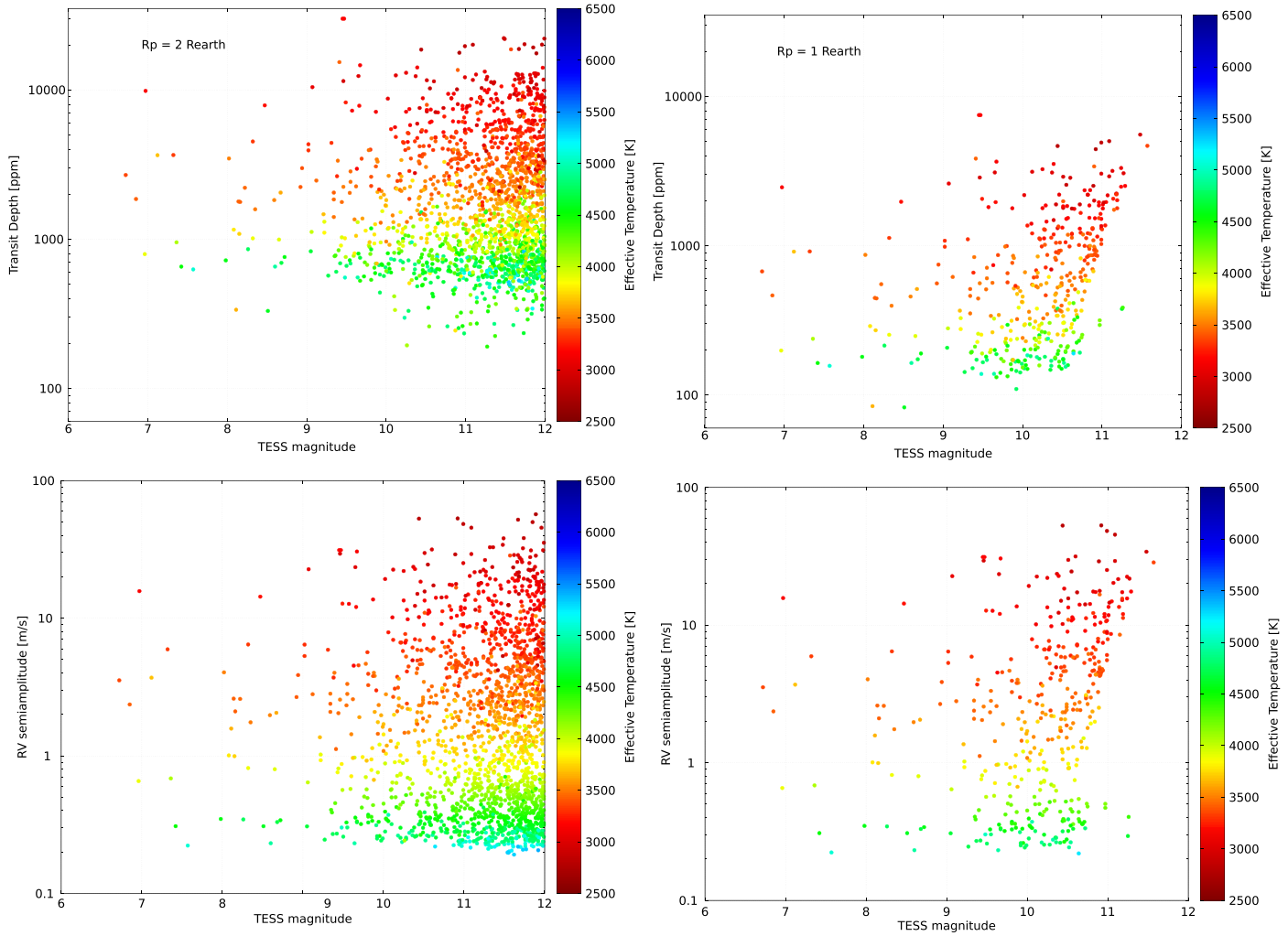

Figure 4. Modeled transit depth (top) for each star of the *TESS* Habitable Zone Star Catalog, where *TESS* can detect a transiting planet of (left) a 2 Earth radii and (right) a 1 Earth radius size during one transit. Modeled radial-velocity semiamplitude K in m s^{-1} (bottom) assuming a 1 Earth mass planet orbiting at a distance where it receives the same radiation as Earth does from the Sun, from its host star.

are not the best template. To detect features in an Earth-analog transmission spectrum (see, e.g., Kaltenegger & Traub 2009; Rauer et al. 2011; Kaltenegger 2017) will require a large telescope, and will be at the limit of technical capability of telescopes already being built like *JWST* (e.g., Deming et al. 2009; Kempton et al. 2018) and the Extremely Large Telescope (ELT; e.g., Snellen et al. 2013; Rodler & Lopez-Morales 2014). Such measurements are a baseline for future mission concepts like those proposed for the decadal survey for 2020.

Upcoming ground-based ELTs are also designed to characterize extrasolar planets. The *TESS* planets will be excellent targets for observations due to the apparent brightness of their host stars. Comparing the angular separation (θ (arcsec) $= a$ (au)$/d$ (pc); where $a =$ planet semimajor axis, $d =$ distance to star system) for the angular separation of the 1 au equivalent distance (Table 1) as well as the empirical Habitable Zone outer limit (Table 2) with the inner working angle (IWA) for a telescope, which describes the minimum angular separation at which a faint object can be detected around a bright star shows whether planets at such orbital distances could be remotely detected and resolved in the near future. For example the 38 m diameter ELT should have an IWA of about 6 mas when observing in the visible region of the spectrum (assuming $\theta_{\rm IWA} \approx 2(\lambda/D)$, where λ is the observing wavelength and D is the telescope diameter).

The apparent angular separation of the outer edge of the empirical HZ of the stars in the *TESS* Habitable Zone Star Catalog is between about 76 and 1.6 mas for the 227 stars, where *TESS* can probe the full HZ for transiting planets. The apparent angular separation of the 1 au equivalent orbital distance around all stars is between 33 and 0.3 mas. Assuming an IWA of 6 mas for the ELT, for 237 of the 1822 stars of the *TESS* Habitable Zone Stars Catalog, a planet at the 1 au equivalent distance could be resolved. Assuming an IWA of 6 mas, for 22 stars, a planet in the empirical HZ of the star could be resolved down to the inner edge of the HZ with ELT.

4. Discussion

4.1. Assumed Observing Time with TESS

Because *TESS* started science observations in 2018 July, the observing times for each star we examine are based on a parameterized estimate from Barclay et al. (2018) based on the ecliptic latitude of the stars and the average number of *TESS* sector observations each star would receive by *TESS* in the 2 yr prime mission lifetime. Note that this parameterization does not

account for whether or not the observations will be continuous; for some host stars, e.g., stars observed in sectors 1 and 13, the observations will cover 54 days; however, as the observing time will not have been undertaken continuously, a transit seen only once in one sector cannot easily be combined with a transit seen only once in the second sector, and such a planet will need to be observed further to determine its orbit. The tables also show whether the star has already been observed in Sectors 1 through 6 of the *TESS* mission.

4.2. Alternative Habitable Zone Limits

There is not one common irradiation limit used throughout the literature for the boundaries of the HZ. This stems from different teams using different irradiation limits for the boundaries of liquid water on the surface of a rocky planet. We focus on the 1 au equivalent flux in this paper and use the empirical HZ limits to explore the sample of stars where *TESS* can observe the full HZ. We use the inner limit being set by the irradiation Venus received when we know it no longer held liquid surface water (RV; see Kasting et al. 1993) assuming N_2–CO_2–H_2O atmospheres. Note that the inner limit is not well known because of the lack of a reliable geological surface history of Venus beyond about 1 billion years due to resurfacing of the stagnant lid, which allows for the possibility of a liquid surface ocean; however, it does not stipulate a liquid ocean surface. Using radiation higher than that limit for the inner edge of a Habitable Zone would have to explain why such planets could maintain their surface water in contrast to Venus (some small irradiation increase can be argued for dry desert planets, see Abe et al. 2011).

Using 3D Global Climate models, the inner edge of the Habitable Zone changes from the empirical value (see Table 1); however, the outer edge of the HZ boundaries for N_2–CO_2–H_2O atmospheres is similar between models. Thus the number of stars where *TESS* can probe the whole HZ does not change when using HZ limits derived from 3D models, because it is determined by the largest period at which *TESS* is sensitive to a transiting planet, set by the furthest distance from the star, which is the outer edge of the HZ. However the boundaries of the HZ and especially the outer edge of the HZ can change with atmospheric composition of the planet (e.g., by adding additional greenhouse gases like H, as discussed, e.g., by Pierrehumbert & Gaidos 2011; Ramirez & Kaltenegger 2017) or CH_4 (Ramirez & Kaltenegger 2018). A lively discussion exists in the literature (see review by Kaltenegger 2017 and references therein) on the influence of rotation rate, cloud coverage, and hazes on the limits of the HZ, using extrapolation of 3D models to different environments. With no clear answer, we have used the empirical HZ in this paper to compare the number of stars where *TESS* can probe the whole HZ for transiting planets to the number of stars where *TESS* can detect planets receiving Earth-analog radiation. Note that being in the HZ does not necessarily mean that a planet is habitable, and in-depth follow-up spectral observations of their atmospheres are needed to characterize planets and search for signs of life (see review Kaltenegger 2017)

4.3. Habitable Planet Yield

While the catalog presented here provides a target list for investigations of the *TESS* stars for a habitable planet search, the actual yield of habitable planets remains unknown and is not the focus of this paper. The number of expected planet detections depends on a number of factors, including the intrinsic occurrence rate of small planets in the habitable zones of these stars, the fortuitous alignment of such planets orbiting stars in the sample we have presented, and the characteristics of the *TESS* data that would allow such transiting planets to be confidently detected, most with a small number of transits seen. Several studies indicate that the occurrence rate of rocky planet in the HZ of cool stars is higher than for hotter stars (see e.g., Dressing & Charbonneau 2013; Petigura et al. 2013); however, the numbers vary between studies. Note that these values have changed due to updates for distances by *Gaia* DR2 (see, e.g., Berger et al. 2018; Johns et al. 2018). Several previous studies have estimated the transiting planet yield for *TESS*. Sullivan et al. (2015) predicts about 14, Bouma et al. (2017) predicts 11, and Barclay et al. (2018) predicts 9 detected planets with radii below 2 Earth radii in the HZ.

Our catalog does not attempt to revisit those calculations, which were based on average calculated stellar and planet distributions that did not include *Gaia* DR2 data. Rather, we provide the specific targets that will be worth special attention by *TESS* and the community in order to focus the search for habitable planets. However, note that the number of stars that can be probed for planets, is not the same as the expected detected planets, the so-called planet yield.

As a very simplified example, assuming a 10% transit probability, a 25% occurrence rate of planets out to 1 au equivalent orbital distance for all stars in our catalog would predict about 10 one-Earth-size planets, detected during one transit. Assuming a 50% occurrence rate would predict 20 one-Earth-size planets out to the 1 au-equivalent distance. For 2 Earth-size radii the number increases to 45 planets out to the 1 au equivalent distance for an occurrence rate of 25%, and 90 transiting planets for a 50% occurrence rate, which *TESS* can detect during one transit. These numbers are only first-order estimates to illustrate the point that the number of stars in the *TESS* Habitable Zone catalog does not equal the number of expected planets. Note that *TESS* can probe the whole HZ for 227 stars brighter than $T = 12$; however, it can probe the HZ partially—out to Earth-equivalent irradiation—for all 1822 stars in the *TESS* Habitable Zone Star Catalog, thus an estimate for expected detection planets in the Habitable Zone would require a detailed model of planet distribution versus orbital distance, which is highly uncertain.

This paper identifies the host stars brighter than $T = 12$, around which *TESS* has the sensitivity to detect transiting planets receiving Earth-like irradiation as well as the subsample where *TESS* can observe the full Habitable Zone and thus can identify planets orbiting at these distances during its prime mission lifetime of 2 yr. Observing the *TESS* Habitable Zone Catalog Stars will give us deeper insight into the occurrence rate of planets, out to Earth-analog irradiation as well as in the Habitable Zone, especially around cool stars.

4.4. Comparison to Other Catalogs Identifying nearby Stars to Search for Exoplanets

Several lists of the closest stellar targets for investigating habitable planets, with stars selected based on proximity, brightness, and other factors exist, e.g., the Catalog of Nearby Habitable Systems (HabCat; Turnbull & Tarter 2003) lists over 17,000 nearby stars, the Target star catalog for Darwin Nearby Stellar sample for a search for terrestrial planets (DASSC; Kaltenegger et al. 2010), which identified the best 1229 single MS stars for follow-up observations, and the Catalog of Earth-Like

Exoplanet Survey Targets (CELESTA; Chandler et al. 2016), which lists 37,000 nearby stars. DASSC and CELESTA also provide habitable zone size estimates.

What distinguishes this catalog from previous work like HabCat, DASSC, and CELESTA is that the stars included here are specifically selected because they are observed with sufficient time by *TESS* to be able to detect two transits of planets that receive similar irradiation to Earth, and that *TESS* can detect planets down to 2 Earth radii during one transit. All of these stars are included in the *TESS* exoplanet Candidate Target List, ensuring that they will also have 2 minute cadence observation (provided they do not fall in *TESS* camera pixel gaps), providing a specific catalog for the *TESS* mission of stars, where the 1 au equivalent distance can be probed for transiting planets.

5. Conclusions

We present the *TESS* Habitable Zone Stars Catalog, a list of 1822 nearby stars with *TESS* magnitude brighter than 12 with reliable *Gaia* DR2 distance. Around these stars *TESS* has the sensitivity to detect two transits of planets, which receive Earth-analog irradiation during the 2 yr prime mission. For all these stars *TESS* has the sensitivity to detect planets down to 2 Earth during one transit. For 408 of these stars, *TESS* can detect transiting planets down to 1 Earth-size during one transit. The catalog stars' effective temperatures are between about 2700 and 5400 K. 137 of these stars are located in the *JWST* continuous viewing zone. 1350 of these stars are located in the 250 days *JWST* viewing zone, $\pm 20^{\circ}$ off the ecliptic poles. For 227 stars in the *TESS* Habitable Zone Stars Catalog, *TESS* can probe the full extent of the Empirical Habitable Zone for transiting planets.

Observing the *TESS* Habitable Zone Catalog Stars will give us deeper insight into the occurrence rate of planets, out to Earth-analog irradiation as well as in the Habitable Zone, especially around cool stars.

Tables 2 and 3 show the stars for which *TESS* can detect two transits for planets at 1 au equivalent distance and the subset of stars where *TESS* can observe planets throughout the whole Habitable Zone, respectively. The tables sort the stars in the *TESS* Habitable Zone Star Catalog by apparent angular separation, showing that the 1 au equivalent distance for hundreds of these stars can be resolved for upcoming ELTs, making them excellent targets for atmospheric characterization in the near future.

ORCID iDs

L. Kaltenegger https://orcid.org/0000-0002-0436-1802
J. Pepper https://orcid.org/0000-0002-3827-8417
K. Stassun https://orcid.org/0000-0002-3481-9052
R. Oelkers https://orcid.org/0000-0002-0582-1751

References

Abe, Y., Abe-Ouchi, A., Sleep, N. H., & Zahnle, K. J. 2011, AsBio, 11, 5
Alonso, R., Brown, T. M., Torres, G., et al. 2004, ApJL, 613, L153
Alsubai, K. A., Parley, N. R., Bramich, D. M., et al. 2013, ACTAA, 63, 465
Andrae, R., Fouesneau, M., Creevey, O., et al. 2018, A&A, 616, A8
Auvergne, M., Bodin, P., Boisnard, L., et al. 2009, A&A, 506, 411
Bailer-Jones, C. A. L. 2015, PASP, 127, 994
Bailer-Jones, C. A. L., Rybizki, J., Fouesneau, M., et al. 2018, AJ, 156, 58
Bakos, G., Noyes, R. W., Kovács, G., et al. 2004, PASP, 116, 266
Barclay, T., Pepper, J., Quintana, E. V., et al. 2018, ApJS, 239, 2
Berger, T. A., Huber, D., Gaidos, E., & van Saders, J. L. 2018, ApJ, 866, 99
Borucki, W. J., Koch, D., Basri, G., et al. 2010, Sci, 327, 977
Bouma, L. G., Winn, J. N., Kosiarek, J., et al. 2017, arXiv:1705.08891
Chandler, C. O., McDonald, I., & Kane, S. R. 2016, ApJ, 151, 59
Clampin, M., JWST Science Working Group, JWST Transits Working Group, Deming, D., & Lindler, D. 2009, Comparative Planetology: Transiting Exoplanet Science with JWST, AST2010 Science White Paper
Deming, D., Seager, S., Winn, J., et al. 2009, PASP, 121, 952
Dressing, C. D., & Charbonneau, D. 2013, ApJ, 767, 1
Fortier, A., Beck, T., Benz, W., et al. 2014, Proc. SPIE, 9143, 91432J
Gaia Collaboration, Brown, A. G. A., Vallenari, A., et al. 2018, A&A, 616, A1
Gaia Collaboration, Prusti, T., de Bruijne, J. H. J., et al. 2016, A&A, 595, A1
Garrett, D., Savransky, D., Belikov, R., et al. 2018, arXiv:1810.02847
Huang, C. X., Shporer, A., Dragomir, D., et al. 2018, arXiv:1807.11129
Huang, C. X., Burt, J., Vanderburg, A., et al. 2019, ApJL, arXiv:1809.05967
Johns, D., Marti, C., Huff, M., et al. 2018, ApJS, 239, 1
Kaltenegger, L. 2017, ARA&A, 55, 433
Kaltenegger, L., Eiroa, C., & Friedlund, M. 2010, Ap&SS, 326, 233
Kaltenegger, L., & Haghighipour, N. 2013, ApJ, 777, 165
Kaltenegger, L., Henning, W., & Sasselov, D. 2010, ApJ, 140, 1370
Kaltenegger, L., & Sasselov, D. 2010, ApJ, 708, 1162
Kaltenegger, L., & Traub, W. A. 2009, ApJ, 698, 519
Kane, S. R., & Hinkel, N. R. 2013, ApJ, 762, 7
Kasper, M. E., Beuzit, J.-L., Verinaud, C., et al. 2008, Proc. SPIE, 7015, 70151S
Kasting, J. F., Whitmire, D. P., & Reynolds, R. T. 1993, Icar, 101, 108
Kempton, E. M.-R., Bean, J. L., Louie, D. R., et al. 2018, PASP, 130, 114401
Kopparapu, R. K., Ramirez, R., Kasting, J. F., et al. 2013, ApJ, 765, 131
Kopparapu, R. K., Ramirez, R. M., Schottel Kotte, J., et al. 2014, ApJL, 787, L29
Leconte, J., Forget, F., Charnay, B., et al. 2013, A&A, 554, A69
Lindegren, L., Hernández, J., Bombrun, A., et al. 2018, A&A, 616, A2
McCullough, P. R., Stys, J. E., Valenti, J. A., et al. 2005, PASP, 117, 783
Muirhead, P. S., Dressing, C., Mann, A. W., et al. 2018, AJ, 155, 4
Oelkers, R. J., Rodriguez, J. E., Stassun, K. G., et al. 2018, AJ, 155, 39
Pierrehumbert, R., & Gaidos, E. 2011, ApJL, 734, L13
Pepper, J., Pogge, R. W., DePoy, D. L., et al. 2007, PASP, 119, 923
Petigura, E. A., Howard, A. W., Marcy, G. W., et al. 2013, PNAS, 110, 19273
Pollacco, D. L., Skillen, I., Collier Cameron, A., et al. 2006, PASP, 118, 1407
Ramirez, R. M., & Kaltenegger, L. 2014, ApJL, 797, L25
Ramirez, R. M., & Kaltenegger, L. 2016, ApJ, 823, 6
Ramirez, R. M., & Kaltenegger, L. 2017, ApJL, 837, 1
Ramirez, R. M., & Kaltenegger, L. 2018, ApJ, 858, 72
Rauer, H., Catala, C., Aerts, C., et al. 2014, ExA, 38, 249
Rauer, H., Gebauer, S., Paris, P. V., et al. 2011, A&A, 529, A8
Ricker, G. R., Vanderspek, R., Winn, J. N., et al. 2016, Proc. SPIE, 9904, 99042B
Rodler, F., & Lopez-Morales, M. 2014, ApJ, 781, 54
Rogers, L. A. 2015, ApJ, 801, 41
Snellen, I., de Kok, R., Le Poole, R., Brogi, M., & Birkby, J. 2013, ApJ, 764, 182
Stassun, K. G., Oelkers, R. J., Pepper, J., et al. 2018, AJ, 156, 102
Sullivan, P. W., Winn, J. N., Berta-Thompson, Z. K., et al. 2015, ApJ, 809, 77
Turnbull, M. C., & Tarter, J. C. 2003, ApJS, 145, 181
Udry, S., & Santos, N. C. 2017, ARA&A, 45, 397
Vanderspeck, R., Huang, C. X., Vanderburg, A., et al. 2019, ApJL, 871, L24
Winn, J. N., & Fabrycky, D. C. 2015, ARA&A, 53, 409
Wolfgang, A., Rogers, L. A., & Ford, E. B. 2016, ApJ, 825, 19